UNIVERSITÀ
DEGLI STUDI
DI PADOVA

DIPARTIMENTO DI INGEGNERIA DELL'INFORMAZIONE

CORSO DI LAUREA IN INGEGNERIA ELETTRONICA

"Reflecting telescope configurations for CubeSat technology"

Relatore: Prof. Corso Alain Jody

Laureanda: Franzato Silvia

ANNO ACCADEMICO 2023-2024

Data di Laurea 19/07/2024

Abstract

In this thesis are shown different configurations for a space reflecting telescope realized with the CubeSat standard, whose aim is to observe sun-grazing comets.

Firstly it is shown how these near-Sun comets can be observed in the UV spectrum, observing the first line of emission of the Hydrogen that is produced from the ice presents on the surface of these comets. Based on the distances of these comets from the hearth, some parameters for the design of the telescope have been calculated.

Then the CubeSat's background is briefly discussed to understand why the decision to use this technology for the design of the telescope has been taken.

The last chapter is dedicated to the structure of the telescope, it is explained the need to use a reflecting telescope. The basic structure and parameters of a telescope are described and the monochromatic aberrations that could affect the images of the telescope are described with the use of the Seidel Sum. The Ritchey-Chrétien configuration of the system is described and the need of an off axis configuration is explained. Then has been made a first order design of the telescope, with the use of paraxial matrices, and then the Spherical and Coma aberrations have been corrected. Two versions of the telescope with slightly different characteristics are proposed.

Ultimately, the necessary coating and the filter to reflect the correct wavelength are described.

Sommario

In questa tesi sono mostrate diverse configurazioni di un telescopio spaziale riflettente che viene realizzato utilizzado lo standard CubeSat, questo telescopio verrà utilizzato per l'osservazione di comete in prossimità del sole.

Inizialmente viene mostrato come queste comete possono essere osservate nello spettro dell'ultravioletto, osservando la prima linea di emissione dell'idrogeno che viene prodotto dal ghiaccio presente sulla superficie delle comete. In base alla distanza delle comete dalla terra sono calcolati i parametri principali per il dimensionamento del telescopio.

Viene mostrato lo standard CubeSat per spiegare i motivi della decisione di utilizzare questa tecnologia per la realizzazione del telescopio.

L'ultimo capitolo viene dedicato alla progettazione del telescopio e viene spiegata la necessità di utilizzare un telescopio in riflessione. La struttura base di un telescopio e i suoi parametri vengono illustrati e vengono descritte attraverso le somme di Seidel le possibili aberrazioni monocromatiche che possono affliggere le immagini del telescopio. Viene descritta la configurazione Ritchey-Chrétien del telescopio e il perché della necessità di utilizzare una configurazione fuori asse del telescopio. Viene poi eseguita un'analisi al primo ordine e viene effettuata la correzione delle aberrazioni sferica e di coma. Vengono proposte due versioni del telescopio con caratteristiche leggermente diverse.

Infine, vengono descritti i coating e il filtro necessari per l'osservazione della lunghezza d'onda desiderata.

Contents

Chapter 1

Introduction

A telescope is an optical element used to observe distant objects, if used on the hearth is called terrestrial and if it is launched into space as a satellite, it is called a space telescope.

Space telescopes are an essential part of space observation since they allow to observe a much broader electromagnetic spectrum than the one observable from the earth.

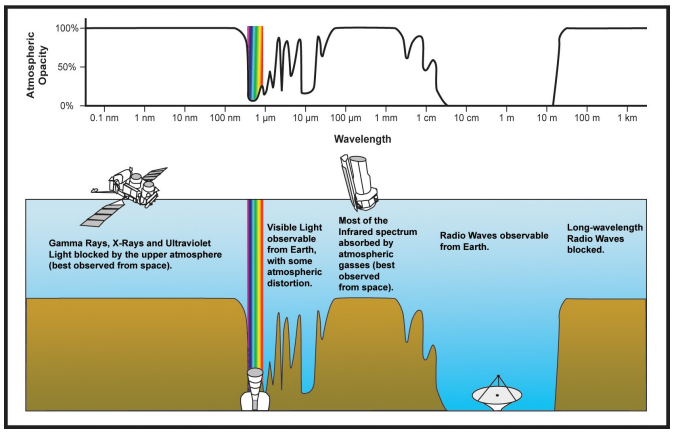

Figure 1.0.1: Atmospheric electromagnetic transmittance
Credit: Public Domain, https://commons.wikimedia.org/w/index.php?curid=1898726

As it is possible to see in the figure above, fig. 1.0.1, Gamma rays, X-rays, Ultraviolet, far infrared and low-frequency radio are completely blocked by the earth's atmosphere. Therefore, these wavelengths cannot be observed from the ground and thus lays the need for space telescopes.

Some example of already launched telescopes in these ranges are: the James Webb telescope, [1], observing in the infrared; the Chandra X-Rays Observatory [2] and AGILE [3] (Astro-Rivelatore Gamma a Immagini Leggero) launched by the Italian Space Agency that are observing in the X-rays. The Ultraviolet and Extreme Ultraviolet are observed by solar telescopes such as: the EIT (Extreme Ultraviolet Imaging telescope for the SOHO Mission) inside

the SOHO satellite [4] (Solar and Heliospheric Observatory), the AIA (The Atmospheric Imaging Assembly on the Solar Dynamic Observatory) and the EUI (Extreme Ultraviolet imaging) inside the Solar Orbiter, [5].

But telescopes are used in space also for wavelengths that are observable from the earth, an example is the Hubble Space telescope, [6]. This is because on earth there could be a reduced visibility for long periods of time due to bad weather. But even with a clear sky there could be defects in the images due to air turbulence in the atmosphere.

Despite the advantages that are achieved using a telescope placed in space rather than one placed on earth, there are major inconveniences associated with the design and the launch of space telescopes. These telescopes can be labour intense and time consuming to design and produce. Typically space telescopes can weight up to hundreds of kilograms with a resulting increase in costs. All things considered, the budget for the design, realization and launch of a space telescope can add up to hundreds million of euros.

But in recent years, a new standard for pico-satellite called CubeSat has opened new possibilities for researchers and students to access space and therefore also a new platform for designing space telescopes. As it will be more analysed later, CubeSats are a very cost effective technology that can be used for various applications. The downside of a space telescope realized with this technology is its limited capability compared to telescopes realized on standard satellites. This is because the reduced volume of these CubeSats is what allows them to be lightweight and therefore more affordable, but it is this characteristic that imposes a limit to the equipment that can be loaded in the pico-satellite.

In this thesis I will show some possible configurations of a reflective space telescope, which can be realized using the CubeSat standard. The need of a space telescope, and therefore the possible application on a CubeSat, comes from the wavelength that is observed, which is 121.6 nm. This wavelength is part of the ultraviolet range that is completely absorbed by the earth's atmosphere and for this reason the telescope must be placed in space.

1.1 Observation of near-sun comets

The space telescope is meant to observe near-Sun comets, but in particular it observes the first line of the emission spectrum of the Hydrogen.

This specific wavelength is observable when comets orbit near the sun. This happens because when comets get heated up by the Sun, the ice presents in the nucleus or in the surrounding grains sublimates into water vapor. The water vapor then get hit by the sun's photons and by

means of photodissociation, Hydrogen is produced. Firstly, the water vapor reacts with the incoming light producing Hydrogen and Hydroxyl, then the Hydroxyl reacts again with the sun's photons and trough a second phenomenon of photodissociation Hydrogen and Oxygen are produced, see fig. 1.1.1a and fig. 1.1.1b

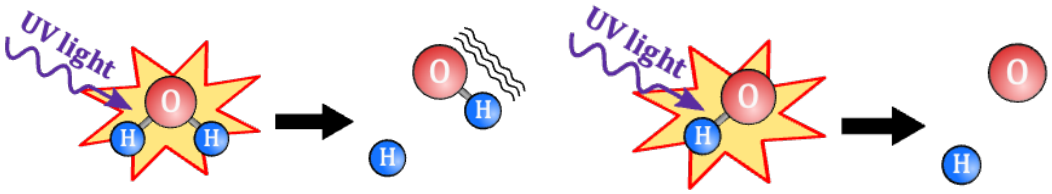

(a) Water photodissociation (b) Hydroxyl photodissociation

Figure 1.1.1: Photodissociation processes
Credit: Alain Jody Corso, Metis Comets Catania

The two phenomena just illustrated can be described by the following reactions:

$$H_2O + h\nu \rightarrow OH + H \tag{1.1.1}$$

$$OH + h\nu \rightarrow O + H \tag{1.1.2}$$

Successively the hydrogen just produced, also gets hit by the sun's photons and a phenomena of resonant scattering occur. The associated emitted wavelength corresponds to the first line of the emission spectrum of the Hydrogen at λ = 121.6 nm. Therefore this wavelength can be associated with orbiting comets, and therefore by observing it, comets can be indirectly observed. An example of the observation in UV of the Comet C/2021 A1 Leonard from the Solar Orbiter can be seen in the following figure.

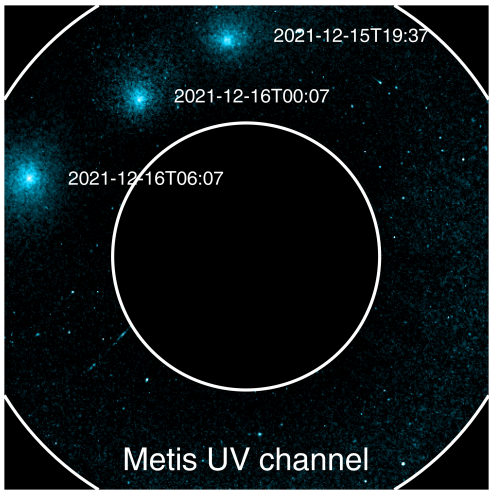

Figure 1.1.2: View of the Comet Leonard in UV from the Solar Orbiter, in three different moments in time
@ESA/Solar Orbiter/Metis Team

This particular wavelength in the UV when observed can also be analyzed and from the intensity of radiation it is possible to determine the amount of water production of the observed comet.

1.1.1 Telescope parameters

The CubeSat telescope once launched can be placed in a Low Earth Orbit (LEO), its distance from the sun can be approximated to around 150M kilometers or around 1 au (Astronomical Unit). The comets that are to be observed at their perihelion, typically have a distance from the hearth of around 70M to 180M kilometers. These comets, when orbiting near the sun, produce a Hydrogen coma that surrounds them that has a typical radius of less than 100K kilometers, this is to consider as the dimension of the object to be observed with the telescope.

Depending on the characteristic of detector used and on the quantity of pixels covered by the image, it is possible to decide a plate scale, and therefore a focal length, for the telescope. It is used a low price detector of 1024 by 1024 pixels, with the pixel dimension of 25 μm by 25 μm. It is decided that a comet should cover around 100 pixels when nearest to the heart.

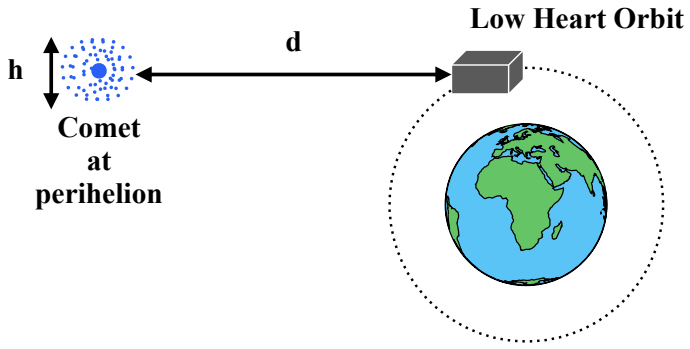

Figure 1.1.3: Scheme of the observation of the comet
Not to scale

Referring the scheme in fig.1.1.3, h represents the dimension of the comet's coma, d represents the distance of the comet from the telescope. Knowing the value of these parameters it is possible to calculate the platescale for the telescope as follow:

$$\Gamma = \frac{h}{d}\frac{1}{\#\text{pixels}} = \frac{2\cdot 10^5}{7\cdot 10^7}\frac{1}{\#\text{pixels}} = 2.86\cdot 10^{-5}\ \text{rad/px}$$
$$= 5.92\ \text{arcsec/px} \simeq 6\ \text{arcsec/px}$$

Ultimately is decided the dimension of the telescope, it should respect the dimension of a 6U CubeSat, 100 mm by 200 mm by 300 mm.

Chapter 2

What are CubeSats

CubeSats are a type of picosatellite designed in 1999 by Professor Jordy Puig-Sauri of California Polytechnic State University (Cal Poly) and Professor Bob Twiggs of Stanford University's Space Systems Development Lab (SSDL). CubeSats are made of multiple 10x10x10 centimeters cubes called units abbreviated as U and that weight up to 2kg each. The purpose of the project was creating a platform to facilitate the access to space to university students; the reduced size of these picosatellites was the key to the success because it permitted to lower costs and time of production.

2.1 Background

Before the CubeSat project was started, space mission were carried by only a few national space agencies with budget of millions of dollars, but the small size of these CubeSats allow them to be added as auxiliary payload in bigger launch vehicles and so drastically reducing once more part of the costs.

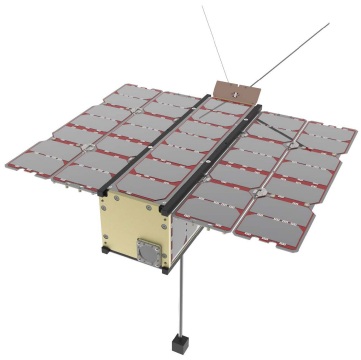

Figure 2.1.1: RadCube a 3U CubeSat
Photo: ©ESA

Moreover the standardised structure permitted over time to produce many off the shelf available

components which permitted a decrease of costs and also allowed everyone to easily obtain basic component to start a project.

CubeSats were designed in 1999 but the first launch happened only in 2003, they were loaded as excess cargo inside the launch vehicle Rockot KS of Eurockot Launch Services. In the following years more CubeSats were produced, however they were mostly designed by spacial agencies and Universities for academic purposes as a tool for student to apply their knowledge or for conducting experiments. But as years passed, they gained more popularity and recently there has been an increase in CubeSats launched by tech company for commercial use such as telecommunication services and hearth observation.

2.1.1 CubeSat Telescope

Another more recent use for CubeSat is astronomical observation so, as I will also show in this thesis, space telescopes are miniaturized to fit inside a multiple Units CubeSat. The first project of this kind was ASTERIA (Arcasecond Space Telescope Enabling Research in Astrophysics) [7] a 6U CubeSat launched in 2017 from the International Space station. Due to that fact that the

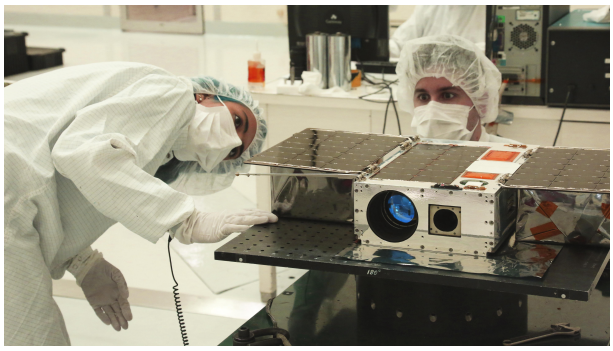

Figure 2.1.2: ASTERIA CubeSat used for exoplanet observation in visible wavelength
Photo:NASA/JPL-Caltech

atmosphere absorbs some part of the electromagnetic field, space telescopes are in high demand because they are designed to cover this portion of spectrum that earth telescopes can't observe. CubeSat telescopes are definitely less accurate than bigger ones but still they are being design because their purpose is different, they are used for longer periods of observation rather than for a single snapshot. In addition having more space telescopes of any capability can enable astronomical researches because they provide more sources of observation.

A possible future application for CubeSat telescopes could be using several of them in co-operation as an autonomous constellation to improve the area that they are able to observe.

2.2 CubeSat Standard

Each CubeSat must be designed accurately and in compliance with the CubeSat Design Specification document (CDS) to make sure of the success and the safety of the CubeSat itself.

The are general specifications, electrical specifications relating to the safety features of the electronic system and operational specifications concerning legal obligation. On the other hand mechanical specifications are in regard of the material selected to build the casing, the rails used to attache the CubeSat to the dispenser, the center of gravity and the weight. In this document can be also found the CubeSat specification drawings that describe the dimensions of the different configurations of CubeSat units that, at the moment, are six as shown in Figure 2.2.1.

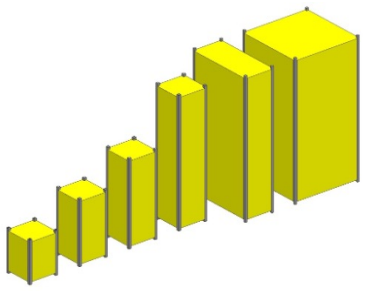

Figure 2.2.1: Possible CubeSat configurations
In order from left to right: 1U, 1.5U, 2U, 3U, 6U, 12U
Credit: From CDS Document

2.3 Launch Mission

One of the most significant aspect of CubeSat is that whoever designs their picosatellite doesn't necessarily have to design a rocket to launch it into space, because they can request to participate to a launch program developed by one of the several launch provider. Usually CubeSats can be added to a launch vehicle of another mission as a secondary payload taking advantage of extra space available. The most used approach is to put the picosatellite inside a dispenser attached to the rockets and expelled it directly from there, but some CubeSats can also be sent to the International Space Station and then released from there.

A typical launch for any spatial mission can be around 100 to 200 millions of euros. Instead, this type of deployment drastically reduced the cost for the launch of the CubeSats, that can be around 100 to 300 thousands of euros. Which in comparison to the budget needed for the a standard launch is substentially more affordable.

2.3.1 Poly Picosatellite Orbital Deployer

The Poly Picosatellite Orbital Deployer (P-POD) is the first deployment system designed for CubeSats by the Cal Poly, it can contain one or more CubeSats but only up to 3 units. The dispenser is a rectangular box with rails inside, a door and a spring mechanism; when CubeSats are released the door opens and the springs push them out of the dispenser. The objective of this deployment system is to attach the CubeSat securely to the rocket, to keep safe the primary load and the CubeSats during the launch and ultimately to release the satellites into space.

Chapter 3

Reflecting telescope

A telescope is an optical system that magnifies the image of a distant object. It can be made of only lenses and it is called a refracting telescope, it can be made only of mirrors and it is called reflecting telescope or it can be made of both lenses and mirrors and it is called catadioptric telescope.

Due to the characteristics needed by the application it is necessary to design a reflecting telescope. The wavelength that is observed with the telescope is $\lambda = 121.6$ nm, which is part of the UV spectrum. The only materials that are transparent at this wavelength are MgF_2 (Magnesium Fluoride) and LiF (Lithium Fluoride). But the Lithium Fluoride is hygroscopic so it absorbs water easily, causing a degradation in the material and therefore it cannot be used.

The only option for a refractive telescope would be to use Magnesium Fluoride, so it is best to opt for a reflecting telescope using Aluminium, since it is a material that has the best reflectance in the UV. This also implies that no chromatic aberrations are introduced in the system and only achromatic aberrations are to be corrected.

3.1 Telescope theory

The are some basic concepts that are the same in every type of telescope.

There is the objective that is the first part of the telescope, it collects the light from the outside and it creates an intermediate image. Then follows the eye piece that takes the image from the objective and it collimates the incoming light to form a virtual image so that it can be seen by the eye. To not lose light between these two components the pupils of these two optical systems must coincide. In this case an object at infinity is conjugate with an image at infinity so there isn't an equivalent focal length, therefore the telescope is called afocal.

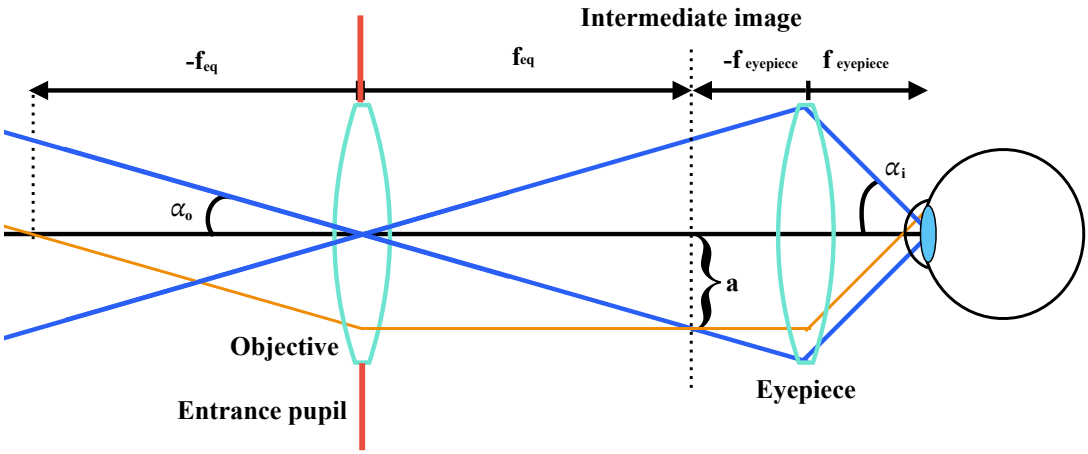

Figure 3.1.1: Example of a telescope with objective and eyepiece

The magnification of the image is described by the ratio of the semi-angle subtended by the object (α_o, see figure 3.1.1) and the semi-angle subtended by the image (α_i, see figure 3.1.1), that is also half of the Field of view:

$$M_P = \frac{\alpha_o}{\alpha_i}$$

Using paraxial approximation the equation above can be rewritten as:

$$\begin{aligned} M_P &= \frac{\tan(\alpha_o)}{\tan(\alpha_i)} \\ &= \frac{f_{eq}}{a} \cdot \frac{a}{f_{eyepiece}} \\ &= \frac{f_{eq}}{f_{eyepiece}} \end{aligned}$$

However the eye piece is not always present, when the telescope is not used by an operator the images are taken by a camera, so the detector can be placed directly on the focal plane of the objective, an example is illustrated in fig. 3.1.2. This particular configuration is used for the design of the CubeSat telescope.

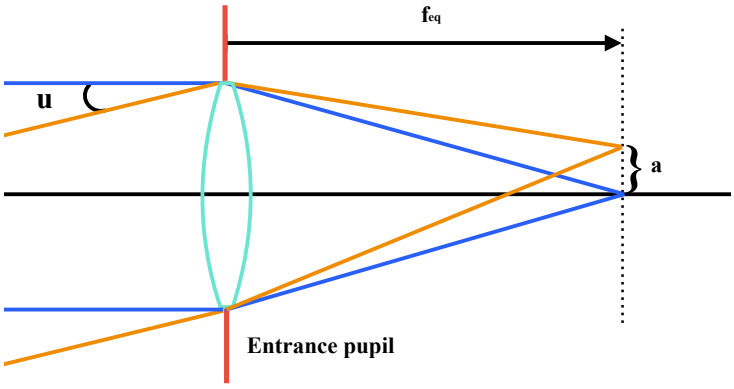

Figure 3.1.2: Example of telescope without eyepiece

When the eyepiece is not present, the magnification is described as Image scale, or Plate scale, which relates the angular size of the Field of view, u see fig. 3.1.2, to the linear size of the image, a see fig. 3.1.2:

$$\begin{aligned} \Gamma &= \frac{\tan u}{a} \\ &= \frac{1}{f_{eq}} \end{aligned} \tag{3.1.1}$$

It possible to understand that with a smaller focal length there are more degrees covered by each pixel and so there is a smaller magnification. Instead with a bigger focal length, less degrees are covered by each pixel so to achieve the same angular coverage more pixels are needed and therefore the image is enlarged.

An other important parameter of a telescope it is the resolving power, it describes the effects on the image of the diffraction from a circular opening. Due to refraction the image of a point source, as for example a star, is a disk called the Airy disk. Therefore to be able to distinguished two different point light sources they must be not too close to each other.
The minimum angular distance of two objects to be resolvable is defined is:

$$\alpha_R = \frac{1.22 \cdot \lambda}{D}$$

The resolving power of the telescope is instead defined as:

$$\rho = \frac{1}{\alpha_r}$$

3.1.1 Achromatic Aberration

Achromatic aberrations are deformations in an object's image. The expected imaged calculated with paraxial optic differs from the actual image formed by the optical system. This is because, in the paraxial approximation are considered only rays with a small angle with respect to the optical axis and rays that are near to it, in this case the approximation of a perfectly stigmatic image is correct. But when analyzing all the rays entering the system, therefore, also crooked rays with respect to the optical axis and rays distant from it, this approximation is incorrect.

Monochromatic aberrations can be characterized by the difference of the actual wave front, observed from the exit pupil, and an ideal spherical wave front, see figure 3.1.3. This wave front difference is called wave front aberration function, which can be expressed by a polynomial function, for every rotational symmetric optical system. The aberrations can also be described

as the different position of the focus point in the image plane, in this case the difference is called transversal aberration.

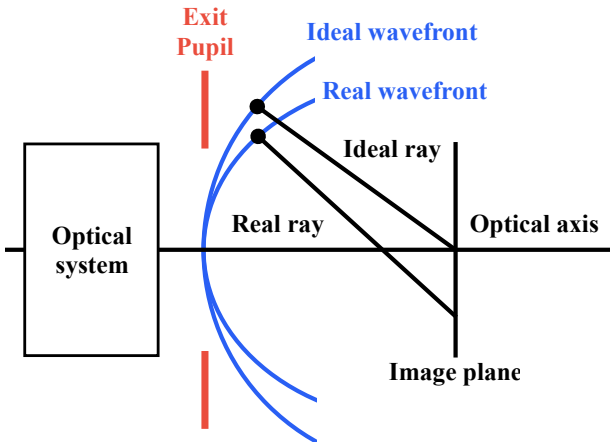

Figure 3.1.3: Difference of real and ideal wavefront

The Seidel sum is a polynomial function which describes this wave front difference for the primary, or first order, aberrations. The primary aberration, also called of third or fourth grade aberrations from the order of the polynomial function of respectively the wave front difference and the transversal aberration, are: spherical aberration, coma aberration, astigmatism, field curvature and distortion.

The incoming rays are characterized by three variables: the height of the ray in the object plane, H, and the position, expressed in circular coordinates, where the ray enters the system in the plane of the entrance pupil, ρ and θ. The exiting rays, instead, can be characterized in terms of wave front difference, W, or Cartesian coordinates in the image plane, TA_x and TA_y.

The Sedidel coefficient are parameters that relate the input rays to the total wavefront difference. Each aberration has his own contribution, that is the sum of the coefficients calculated for each optical surface of the system.

The wave front aberration function, in terms of these Seidel parameters, is:

$$W(H,\rho,\theta) = \frac{1}{8}S_I\rho^4 + \frac{1}{2}S_{II}H\rho^3\cos\theta + \frac{1}{2}S_{III}H^2\rho^2\cos^2\theta + \frac{1}{2}S_V H^3\rho\cos\theta + \frac{1}{4} + (S_{III}+S_{IV})H^2\rho^2 \quad (3.1.2)$$

When using aspherical surfaces auxiliary terms must be added $S_I^*, S_{II}^*, S_{III}^*, S_V^*$.

The transversal difference of the images point can be expressed in terms of the wave front difference expressed in Cartesian coordinates and the radius of the wavefront, R:

$$TA_x = -R\frac{\partial W}{\partial x} \qquad TA_y = -R\frac{\partial W}{\partial y}$$

The Seidel coefficient are calculated from the characteristic of the marginal ray and the chief ray, respectively represented by values with an over line and without the over line.
Referring the image below, 3.1.4, the three parameters are defined as follow:

$$A = ni = n(u + yC) = n'i' \tag{3.1.3}$$

$$B = n\bar{i} = n(\bar{u} + \bar{y}C) = n'\bar{i'} \tag{3.1.4}$$

$$L = n(\bar{u}y - u\bar{y}) \tag{3.1.5}$$

Referring the image below, u is the angle between the optical axis and the ray, i is the angle between the tangent to the surface and the ray and C is equal to $\frac{1}{R}$, where R is the radius of the surface.

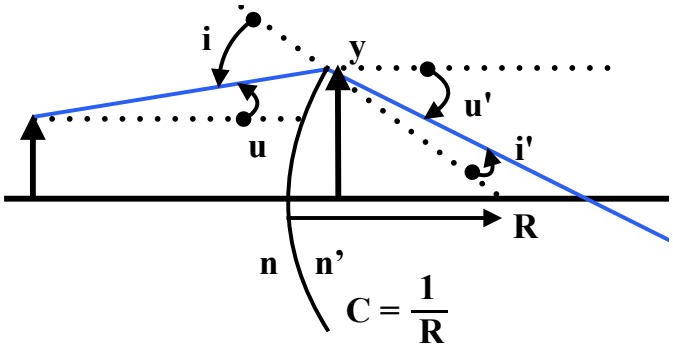

Figure 3.1.4: Marginal ray for a generic optical surface

Spherical abberation

The spherical aberration is the only achromatic aberration that affects also rays that are parallel to the optical axis. This aberration is caused by the change of the focal length with the distance from the axis of the incoming rays, see fig.3.1.5. This causes the image of point light source to be a blurred disk. The shape of the spot changes with the position of where it is observed.

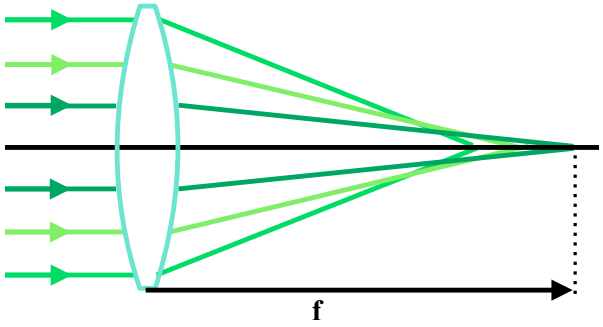

Figure 3.1.5: Change of focal length with the height of the rays

The curve that describes the envelope of the refracted rays is called caustic, it is possible to observe that the minimum spot, also called circle of least confusion, is not placed on the image focal plane but on the intersection of the caustic and the marginal ray.
The Seidel coefficients for spherical aberration are:

$$S_I = -\sum A^2 y \Delta \left\{\frac{u}{n}\right\} \qquad S_I^* = -\sum KC^3 y^4 \Delta\{n\}$$

Coma aberration

Coma is an achromatic aberration that causes the deformation of the image for rays that are tilted with respect to the optical axis. This phenomenon is caused by the different magnifications of object points that enter the system at different heights, see fig. 3.1.6a. This causes the image of a point light source to have a comet shape, see fig. 3.1.6b.

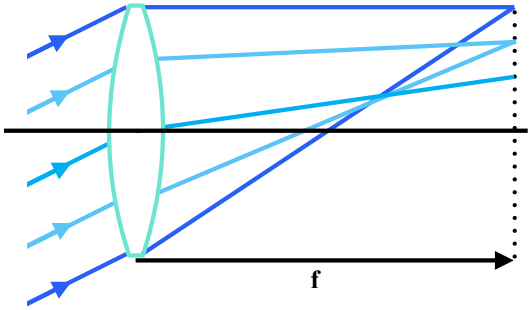

(a) Change of magnification with the distance from the axis

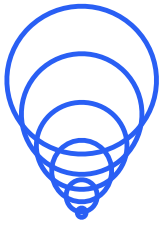

(b) Image of a point source

Figure 3.1.6: Coma aberration

The Seidel coefficients for Coma aberration are:

$$S_{II} = -\sum ABy \Delta \left\{\frac{u}{n}\right\} \qquad S_{II}^* = -\sum KC^3 y^4 \Delta\{n\} \frac{\overline{y}}{y}$$

Astigmatism

Astigmatism occurs when the light source does not lay on the optical axis, therefore the rays enter the system asymmetrically.
The focal length on the sagittal and tangential planes are different. Therefore the circular section of a set of rays is deformed, first is stretched to form an oval and then a segment where the focus of the sagittal plane is placed, see T in figure 3.1.7. Then the section returns to form an oval, in the place of the focus of the tangential plane the rays are again aligned in a segment, S in figure 3.1.7, then the rays form an oval. Between the two focuses of the two planes is positioned the circle of least confusion, which is the smallest spot of the beam.
The Seidel coefficients for astigmatism are:

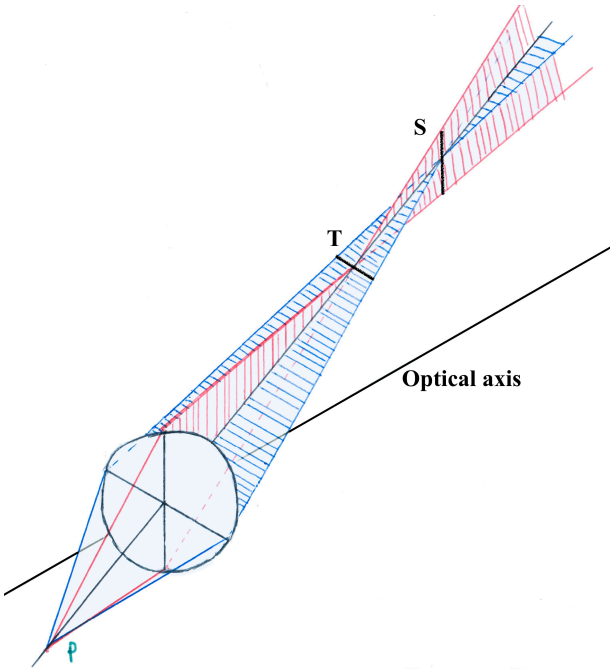

Figure 3.1.7: Astigmatism

$$S_{III} = -\sum B^2 y \Delta \left\{ \frac{u}{n} \right\} \qquad S^*_{III} = -\sum K C^3 y^4 \Delta\{n\} \left(\frac{\overline{y}}{y} \right)^2$$

Field curvature

In an optical system, the image plane is approximated to a plane, but this is true only for a small portion of space near the optical axis. In fact, the stigmatic image plane is a curve, not a plane, therefore the image presents an aberration called field curvature, see figure below, figure 3.1.8

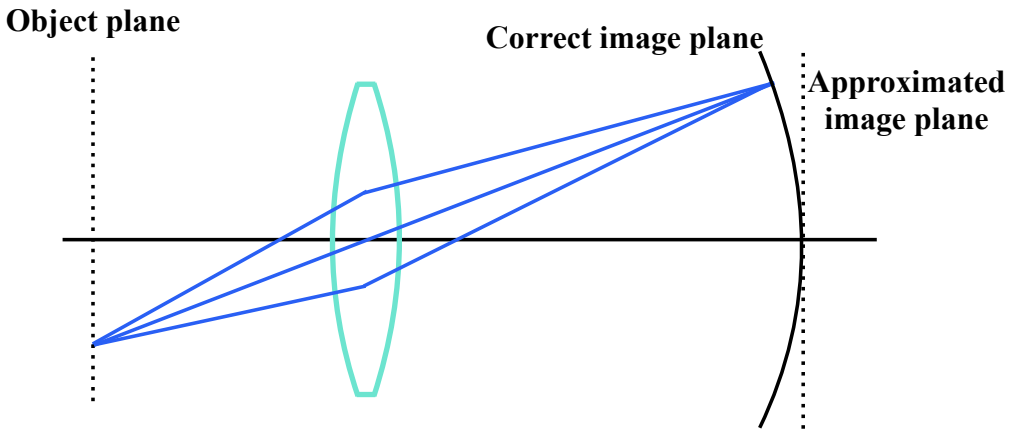

Figure 3.1.8: Field curvature

When in the system astigmatism has been corrected, the curvature is called Petzval and the curvature results the same for both the sagittal and tangential planes.
The Seidel coefficient, for the Petzval curvature, is:

$$S_{IV} = -L^2 \sum C\Delta \left\{\frac{1}{n}\right\}$$

The Petzaval curvature can be corrected with a flattener lens, a plano-concave lens, which extend the optical patch for the rays increasingly more distant from the axis.

Distortion

Distortion is an achromatic aberration that is caused by the different focal length with respect to the off axis distance, therefore different point of the object have different magnification. Referring figure 3.1.9, the distortion can be positive 3.1.9b or negative 3.1.9c, respectively the magnification increase or decrease with the off axis distance of the object.

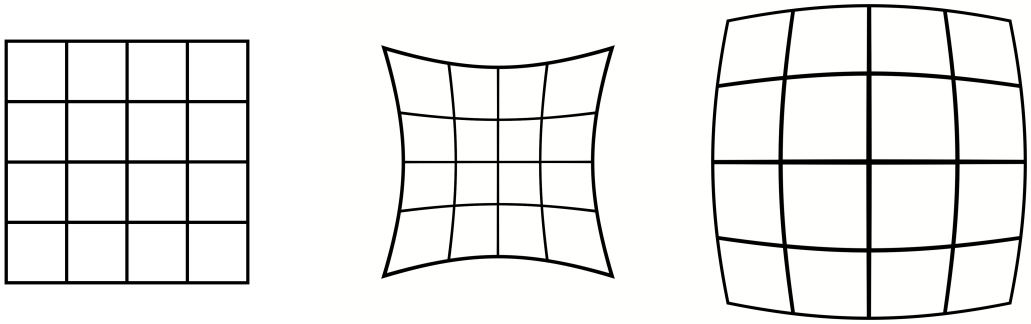

(a) No distortion (b) Positive distortion (c) Negative distortion

Figure 3.1.9: Image of grid with and without distortion

The Seidel coefficients for distortion are:

$$S_V = -\sum \frac{B}{A}\left[CL^2\Delta\left\{\frac{1}{n}\right\} - B^2 y\Delta\left\{\frac{u}{n}\right\}\right]$$

$$S_V^* = -\sum KC^3y^4\Delta\{n\}\left(\frac{\overline{y}}{y}\right)^3$$

Aberration in a two mirror telescope

The Seidel sums can be calculated for a two mirror system, such as a telescope, using paraxial matrices. The resulting Seidel sums for the primary aberrations S_I, S_{II} and S_{III} are:

$$S_I = 1 + k_1 - \left[k_2 + \left(\frac{M+1}{M-1}\right)^2\right] \frac{(M-1)^3 A}{M^3} \tag{3.1.6}$$

$$S_{II} = \frac{2}{M^2} + \left[k_2 + \left(\frac{M+1}{M-1}\right)^2\right] \frac{(M-1)^3(1-A)}{M^3} \tag{3.1.7}$$

$$S_{III} = \frac{4(M-1+A)}{M^2 A} - \left[k_2 + \left(\frac{M+1}{M-1}\right)^2\right] \frac{(M-1)^3(1-A)^2}{M^3 A} \tag{3.1.8}$$

M corresponds to the focal magnification, see equation 3.2.10; A is the first term of the equivalent matrix of the system, see equation 3.2.1; k_1 and k_2 are the conic constant of the two mirrors By zeroing one of these terms the wave front difference between the ideal and actual wave front is removed for that particular aberration. Therefore it is possible to eliminate that particular aberration from the system.

These Seidel sums will be used during the design of the telescope to correct some aberrations that affect the system.

3.2 Telescope configuration

For the design of the CubeSat telescope, as already explained, the only configuration that is possible to apply for the purpose of this telescope is a reflecting configuration, due to the wavelength that needs to be observed.

A Reflecting telescope can be made of two or more mirrors, in this application two mirrors are used, see figure 3.2.1, they are called respectively primary and secondary.

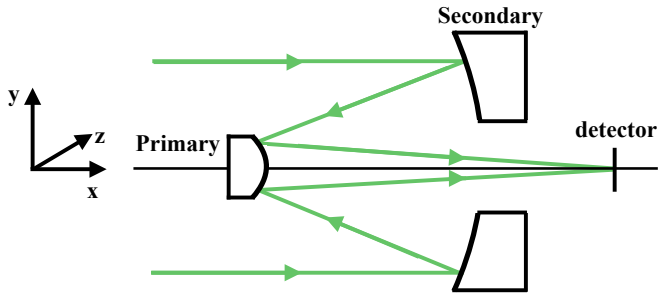

Figure 3.2.1: Example of a reflecting telescope with two mirrors
Not to scale

A reflecting telescope also does not introduce chromatic aberrations and it tends to be easier to mount, since a mirror can be attached from the back.

The reflecting telescope that is most suitable for this application is a Ritchey-Chrétien configuration. The Ritchey-Chrétien is an aplanatic telescope made of two hyperbolic mirrors and it does not present coma or spherical aberration. This configuration also reduces the size of the telescope and therefore it is possible to fit it in the limited volume of the CubeSat.

The CubeSat application indeed sets limits on the dimension and the placement of the two mirrors. Using the reference system sets on the figure 3.2.1, on the x dimension is placed the longer side of the CubeSat to be able to place the two mirrors as far as possible on opposite sides. Then the z dimension is placed on the shortest side of the CubeSat and this creates a limit for the dimension of the two mirrors. Ultimately the y axis represent the 200 mm side of the CubeSat and it sets a limit for the off-axis placement of the mirrors that will be introduced later.

To design the telescope and calculate the main parameters of the optical elements, it has firstly made a first order, or paraxial, analysis of the system using paraxial matrices. The system is perfectly stigmatic when analyzed at the first order, to consider the effect of aberrations and to correct them is necessary to then proceed with a separate analysis of higher grade.

3.2.1 Paraxial design

The telescope can be represented as in the figure below, 3.2.2:

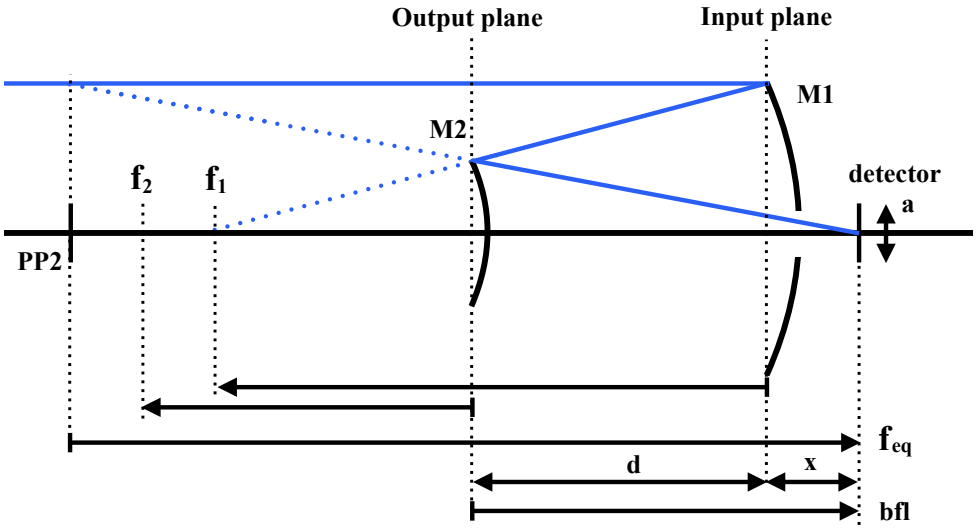

Figure 3.2.2: Scheme of the telescope
Not to scale

The equivalent paraxial matrix of the system is calculated. The system is formed by two mirror matrices and a translation matrix, where the first mirror is the input plane and the secondary is the output plane:

$$\text{First mirror : } \begin{pmatrix} 1 & 0 \\ -\frac{1}{f_1} & 1 \end{pmatrix} \qquad \text{Translation : } \begin{pmatrix} 1 & d \\ 0 & 1 \end{pmatrix} \qquad \text{Second mirror : } \begin{pmatrix} 1 & 0 \\ -\frac{1}{f_2} & 1 \end{pmatrix}$$

The equivalent matrix of the system can be calculated by multiplying the matrix altogether:

$$\begin{aligned} M_{eq} &= \begin{pmatrix} 1 & 0 \\ -\frac{1}{f_2} & 1 \end{pmatrix} \begin{pmatrix} 1 & d \\ 0 & 1 \end{pmatrix} \begin{pmatrix} 1 & 0 \\ -\frac{1}{f_1} & 1 \end{pmatrix} = \begin{pmatrix} 1 & d \\ -\frac{1}{f_2} & -\frac{d}{f_2}+1 \end{pmatrix} \begin{pmatrix} 1 & 0 \\ -\frac{1}{f_1} & 1 \end{pmatrix} = \\ &= \begin{pmatrix} 1-\frac{d}{f_1} & d \\ -\frac{1}{f_2}+\frac{d}{f_2 f_1}-\frac{1}{f_1} & 1-\frac{d}{f_2} \end{pmatrix} \end{aligned} \tag{3.2.1}$$

In this system the back focal length is equal to the sum of the distance between the two mirrors and the distance of the focus from the first mirror.

$$bfl = x + d \tag{3.2.2}$$

The back focal length in this case also represents the space occupied by the telescope, so it should be less then the entire space available in the x dimension to leave room for the mounting

of the mirrors. Using paraxial matrix theory, the back focal length can be calculated also as:

$$bfl = -\frac{A}{C} \tag{3.2.3}$$

Combining equations 3.2.2 and 3.2.3 the following equation can be obtained:

$$\begin{aligned} d + x &= -\frac{A}{C} \\ &= \left(1 - \frac{d}{f_1}\right) f_{eq} \end{aligned} \tag{3.2.4}$$

From 3.2.4 the focal length of the first mirror can be calculated, but first the equivalent focal length of the system must be calculated from the specification of the plate scale.
The plate scale is expressed in arcsec/px but it can be expressed in rad/mm, assuming l is the width of one pixel of the sensor, the equation to change the unit of measurements is:

$$\Gamma \text{ [rad/mm]} = \Gamma \text{ [arcsec/px]} \cdot \frac{\pi}{648000} \cdot \frac{1}{l} \tag{3.2.5}$$

Now is possible to calculate f_{eq} inverting equation 3.1.1:

$$f_{eq} = \frac{1}{\Gamma} \tag{3.2.6}$$

The f/# of the system can now be calculated using the results obtained in the equation 3.2.6 and knowing that the entrance pupil of a telescope is the primary:

$$f/\# = \frac{f_{eq}}{D_1} \tag{3.2.7}$$

Using the result of equation 3.2.6 and 3.2.4 the focal length of the first mirror can be calculated:

$$\begin{aligned} d+x &= \left(1 - \frac{d}{f_1}\right) f_{eq} \\ f_1 &= \frac{d f_{eq}}{f_{eq} - (d + x)} \end{aligned} \tag{3.2.8}$$

The value of the radius of the mirror can be calculated as:

$$R_1 = -2 f_1 \tag{3.2.9}$$

Knowing the value of f_{eq} and f_1 it is possible to calculate the value of the focal magnification:

$$M = \frac{f_{eq}}{f_1} \tag{3.2.10}$$

The focal magnification can also be expressed in terms of f_1, f_2 and d.
Starting from the equivalent matrix of the system is possible to calculate f_{eq} as:

$$\begin{aligned} f_{eq} &= -\frac{1}{C} \\ f_{eq} &= -1/\left(-\frac{1}{f_1} + \frac{d}{f_1 f_2} - \frac{1}{f_2}\right) \\ f_{eq} &= \frac{f_1 f_2}{f_1 + f_2 - d} \end{aligned} \tag{3.2.11}$$

In the equation above, 3.2.11, the focal magnification is defined as:

$$M = \frac{f_2}{f_1 + f_2 - d} \tag{3.2.12}$$

The value of the focal magnification obtained in 3.2.10 and the result obtained in equation 3.2.12 can be used to calculate the value of the focal length of the second mirror:

$$f_2 = \frac{M}{1 - M}(f_1 - d) \tag{3.2.13}$$

The light hits the second mirror from right to left and therefore the sign convention results inverted, to calculate the radius of the second mirror in the correct sign convention the result must be multiply by -1:

$$R_2 = -1 \cdot (-2f_2) \tag{3.2.14}$$

The diameter of the secondary can be calculated tracing the marginal ray, the graphical representation can be seen in the figure below.

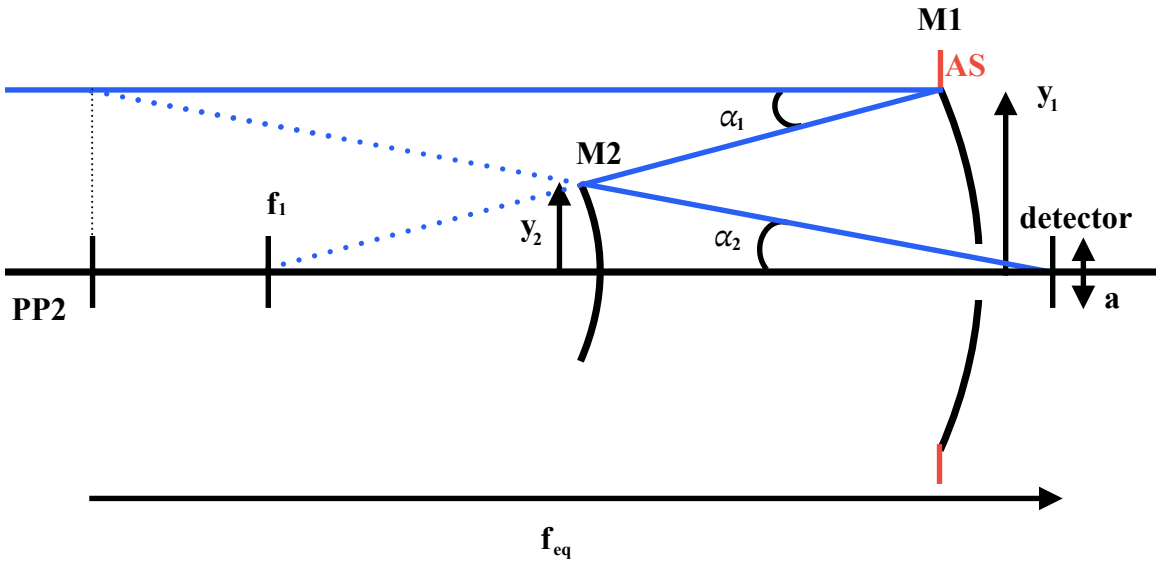

Figure 3.2.3: Tracing of the marginal ray
Not to scale

Using paraxial matrices the marginal ray can be described as:

$$\begin{aligned}\begin{pmatrix} y_2 \\ \alpha_2 \end{pmatrix} &= \begin{pmatrix} 1 & d \\ 0 & 1 \end{pmatrix} \begin{pmatrix} 1 & 0 \\ -\frac{1}{f_1} & 1 \end{pmatrix} \begin{pmatrix} y_1 \\ \alpha_1 \end{pmatrix} \\ &= \begin{pmatrix} 1 - \frac{d}{f_1} & d \\ -\frac{1}{f_1} & 1 \end{pmatrix} \begin{pmatrix} y_1 \\ \alpha_1 \end{pmatrix} \end{aligned} \tag{3.2.15}$$

In the equation above, 3.2.15, y_1 corresponds to the highest point of the primary, so $y_1 = \frac{D_1}{2}$, y_2 corresponds to the highest point of the secondary, so $y_2 = \frac{D_2}{2}$ and α_1 corresponds to half of the field of view.

The field of view can be calculated from the value of the equivalent focal length, f_{eq}, the width of a pixel, l, and the dimension of the detector, a:

$$a = l \cdot 1024 \tag{3.2.16}$$

$$\tan(FoV) \simeq FoV = \frac{a}{f_{eq}} \tag{3.2.17}$$

From equation 3.2.15 and the result of equation 3.2.17 it is possible to obtain the dimension of the secondary:

$$y_2 = \left(1 - \frac{d}{f_1}\right) y_1 + d\alpha_1$$

$$\frac{D_2}{2} = \left(1 - \frac{d}{f_1}\right)\frac{D1}{2} + d\frac{FoV}{2}$$
$$D_2 = 2\left[\left(1 - \frac{d}{f_1}\right)\frac{D1}{2} + d\frac{FoV}{2}\right]$$

The first order design ends here, to calculate the conic constants of the two mirrors it is necessary to describe also non paraxial rays to understand the effects of aberrations.

3.2.2 Aberration correction

In the Ritchey-Chrétien configuration, coma and spherical aberrations are canceled.
In the system there are still two free parameters that have not been calculated which are the conic constants of the two mirrors. Therefore these parameters can be used to correct two aberrations, spherical and coma.
Using the Seidel sums of the primary aberrations S_I and S_{II} for a two mirror system, see equations 3.1.7 and 3.1.6, it is possible to calculate k_1 and k_2, by zeroing the two terms.
By zeroing the coefficient of coma, 3.1.7, it is possible to calculate the value of the conic constant of the second mirror:

$$\frac{2}{M^2} + \left[k_2 + \left(\frac{M+1}{M-1}\right)^2\right]\frac{(M-1)^3(1-A)}{M^3} = 0$$
$$k_2 = -\frac{(M+1)^2}{(M-1)^2} - \frac{2M}{(M+1)^3(1-A)} \tag{3.2.18}$$

From the coefficient of spherical aberration 3.1.6 it is possible to obtain the conic constant of the primary:

$$1 + k_1 - \left[k_2 + \left(\frac{M+1}{M-1}\right)^2\right]\frac{(M-1)^3 A}{M^3} = 0$$
$$k_1 = \left[-\frac{(M+1)^2}{(M-1)^2} - \frac{2M}{(M+1)^3(1-A)} + \left(\frac{M+1}{M-1}\right)^2\right]\frac{(M-1)^3 A}{M^3} - 1$$
$$k_1 = \frac{-2A}{M^2(1-A)} - 1 \tag{3.2.19}$$

3.2.3 Off-axis configuration

A problem that occurs using a typical two mirror telescope, such as the one just designed, is the obstruction that the second mirror creates on the primary. Some part of the incoming light that should hit the primary gets stopped by the secondary, see fig. 3.2.4a .

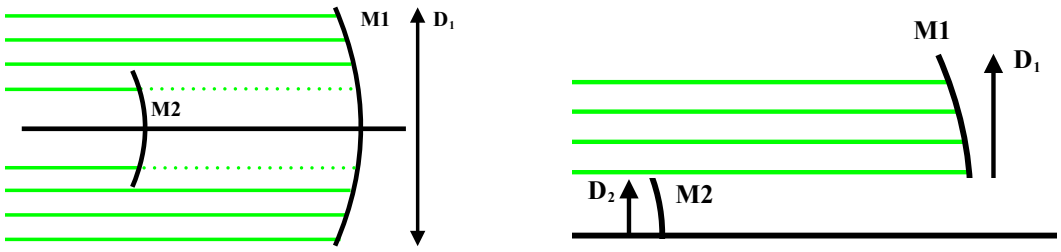

(a) The secondary creates a shadow on the primary (b) Off-axis configuration

Figure 3.2.4: Not to scale

The obstruction that the secondary creates on the primary also causes the figure of diffraction to be bigger. Therefore the resolving power of the telescope is smaller than expected.

To avoid this problem, the solution is to realize an off-axis configuration of the Ritchey-Chrétien. The primary and secondary mirrors are not placed one in front of the other and so the second mirror does not create a shadow on the primary. To do so it is necessary that the mirrors are realized using the upper half of the respective hyperbola.

By referring the image 3.2.4b the height of the primary is called D_1 and the height of the secondary is called D_2. The secondary must be D_2 mm tall and to not create a shadow on the first mirror the primary must be raised from the axis. Therefore the section of the hyperbola used for the primary, has to start at a height of D_2 mm from the axis and the mirror has to be D_1 mm tall.

The paraxial analysis made for the on axis configuration is correct also for this design. Therefore the formulas used to calculated all the parameters in the first configuration can still be used for the design of the telescope for this off axis configuration.

The only change to make, is the equation utilized to calculate the height of the secondary, since is used the trace of the marginal ray and for this configuration the path of that ray is different.

Considering the following scheme of the off-axis configuration of the telescope:

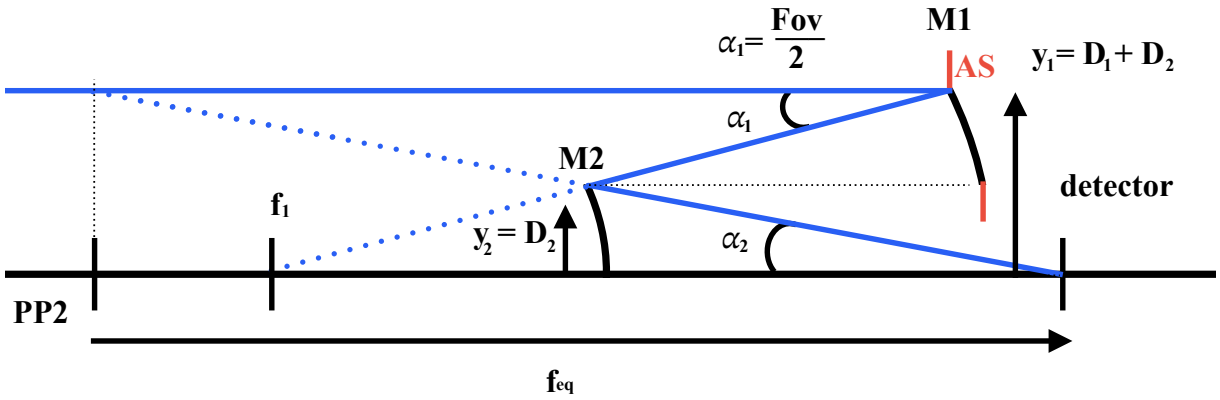

Figure 3.2.5: Marginal ray of the of axis configuration
Not to scale

Using paraxial matrices the marginal ray can be described as:

$$\begin{aligned}\begin{pmatrix} y_2 \\ \alpha_2 \end{pmatrix} &= \begin{pmatrix} 1 & d \\ 0 & 1 \end{pmatrix} \begin{pmatrix} 1 & 0 \\ -\frac{1}{f_1} & 1 \end{pmatrix} \begin{pmatrix} y_1 \\ \alpha_1 \end{pmatrix} \\ &= \begin{pmatrix} 1-\frac{d}{f_1} & d \\ -\frac{1}{f_1} & 1 \end{pmatrix} \begin{pmatrix} y_1 \\ \alpha_1 \end{pmatrix}\end{aligned} \tag{3.2.20}$$

In the equation above, 3.2.20, y_1 corresponds to the highest point of the primary, so $y_1 = D_1 + D_2$, y_2 corresponds to the diameter of the secondary and α_1 corresponds to half of the field of view. From equation 3.2.20 it is possible to obtain the dimension of the secondary:

$$\begin{aligned} y_2 &= \left(1 - \frac{d}{f_1}\right) y_1 + d\alpha_1 \\ D_2 &= \left(1 - \frac{d}{f_1}\right) (D_1 + D_2) + d\frac{FoV}{2} \\ D_2 &= \left[\left(1 - \frac{d}{f_1}\right) D_1 + d\frac{FoV}{2}\right] \left(\frac{f_1}{d}\right) \end{aligned} \tag{3.2.21}$$

3.3 First configuration

A first proposal for a design of the telescope can be made using the formulas derived in a previous sections Paraxial design [3.2.1], Aberration correction [3.2.2] and from the result of equation 3.2.21 for the off-axis configuration.

The telescope, as already decided before, is an off-axis Ritchey-Chrétien two mirror configuration. A scheme of the telescope can be seen in the following figure:

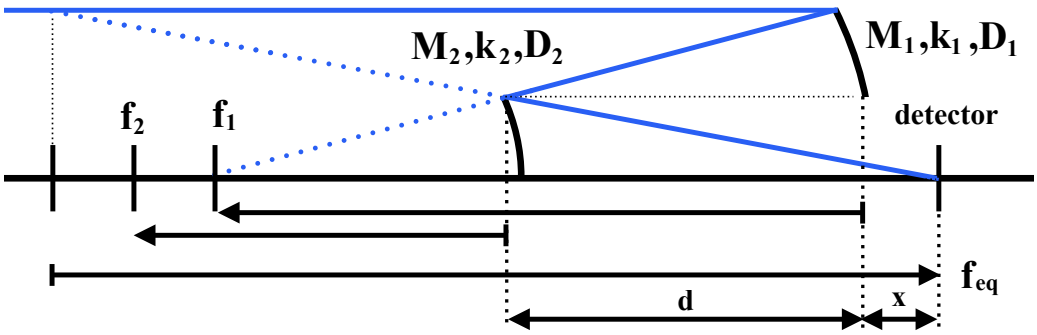

Figure 3.3.1: Scheme of the telescope
Not to scale

The parameters given for the design are the following:

Pixel dimension : 25 µm x 25 µm

Active pixels : 1024 x 1024

Γ : 6 arcsec/px

Primary mirror (D_1) : 70 mm

Dimension : 6U, 100 x 200 x 300 mm

To be able to respect the limitation for the dimension of the telescope, in this first design as a parameter it has been decided the value of the maximum diameter of the primary, to make sure that the mirror could be fitted inside the CubeSat.
All the parameters needed for the design of the telescope are calculated:

$d = 200$ mm	$x = 50$ mm	$f_{eq} = 859$ mm
$f_1 = 282$ mm	$f_2 = -122$ mm	$R_1 = -564$ mm
$R_2 = -224$ mm	$D_1 = 70$ mm	$D_2 = 32.9$ mm
$k_1 = -1.09$	$k_2 = -4.91$	$f/\# = 12.3$

3.4 Second configuration

A second configuration is proposed. The given parameters are:

Pixel dimension : 25 μm x 25 μm

Active pixels : 1024 x 1024

Γ : 7 arcsec/px

f/# : f/10

Dimension : 6U, 100 x 200 x 300 mm

A few different decision on the parameters have been made. The distance between the two mirrors has been reduced and so the telescope occupies a smaller volume. As a parameters has been given the $f/\#$ of the system instead of the diameter of the primary, so after the equivalent focal length has been calculated the dimension of the first mirror is determine knowing the $f/\#$ of the system:

$$f/\# = \frac{f_{eq}}{D_1}$$
$$D_1 = \frac{f_{eq}}{f/\#} \tag{3.4.1}$$

It is important to check that dimension of the mirror respect the specification on the dimension of the system otherwise some parameters of the telescope must be changed.
The parameters calculated are:

$d = 180$ mm	$x = 20$ mm	$f_{eq} = 736$ mm
$f_1 = 247$ mm	$f_2 = -101$ mm	$R_1 = -494$ mm
$R_2 = -202$ mm	$D_1 = 73.6$ mm	$D_2 = 31.7$ mm
$k_1 = -1.08$	$k_2 = -5.08$	

The diameter of the primary results slightly bigger than the one on the first configuration but it's still acceptable. From the results obtained in the second design it is also possible to notice that this system has a shorter focal length then the first design, this results in a smaller magnification. Also the value of the $f/\#$ results smaller then the one of the previous design, therefore more light can enter this system.

3.5 Coating and filter

The telescopes just designed in section 3.3 and 3.4, are to be realized using particular mirrors that are able to reflect the desired wavelength in the Ultraviolet spectrum. To be able to reflect the most of the entering radiation, the mirrors of the telescope should be made of a layer of Aluminium deposited on a substrate, since Aluminium has the best reflectance in the UV. Depending on the deposition condition, the reflectance of the Aluminium changes, but for wavelength shorter than 160 nm also the presence of impurities, like Al_2O_3 (Aluminium oxide), can reduce the reflectance of the film [8]. Therefore the Aluminium film must be protected with a transparent coating. This transparent coating should be made of Magnesium Fluoride since, as explained before, is the only suitable transparent material at this wavelength. This film of Magnesium Fluoride is also realized to have a thickens that realize constructive interference from the film itself, at this wavelength the thickness is around 25 nm.
A mirror realized with a layer of Aluminium and the protective coating of Magnesium Fluoride has a reflectance for the wavelength at 121.6 nm of around 80%, [8].

In the telescope it must be also added a filter to be able to select and observe only the desired wavelength at 121.6 nm. This filter is needed to block all the other wavelengths that could enter the telescope but are not needed to observe the comets. Therefore, the filter should be the size of the primary mirror and placed in front of it so to filter all the entering light. This filter acts like a band pass filter with a transmission peak at around 121 nm, so the only light that will actually enter the telescope is of the correct wavelength. The filter realized with multi-layers of Aluminium and Magnesium Fluoride has a transmittance of around 20%, [8].

Considering that the light is reflected twice inside the mirror, it is possible to calculate an estimate of the percentage of radiation that arrives at the detector:

$$I_{DET} = 80\% \cdot 80\% \cdot 20\% \cdot I_{IN} = 12.8\%\ I_{IN}$$

Chapter 4

Conclusion

In this thesis I described the possible application of a telescope realized inside a CubeSat whose mission is to observe near-Sun comets in the UV spectrum. I showed the necessity for this telescope to be launched into space and the necessity to work in reflection and not transmission. Ultimately, I designed the telescope at the first order and showed different configurations for the telescope.

In writing this thesis I had the opportunity to apply the knowledge acquired in a previous course of ”Elements of Optics and applications”, by paraxially design a small telescope.

But I have also had the opportunity to learn about innovative technology, such as the CubeSats, how their invention has been opening new possibilities for space application such as the telescope discussed in this work. Moreover I have also learned the challenges of working in the UV spectrum, having restricted possibilities of materials with a good reflectivity or transparency and the necessity to observe these wavelengths from space.

I have also been able to start learning a few things about space observation and space application, a new topic for me, and how comets can be observed not only in the visible spectrum but also in the UV by their coma.

Bibliography

1. *Telescope Overview* https://webbtelescope.org/news/webb-science-writers-guide/telescope-overview.
2. *Chandra X-ray Observatory* https://www.nasa.gov/mission/chandra-x-ray-observatory/.
3. *AGILE - Astro-rivelatore Gamma a Immagini Leggero* http://agile.rm.iasf.cnr.it.
4. *ESA - SOHO overview* https://www.esa.int/Science_Exploration/Space_Science/SOHO/SOHO_overview.
5. *ESA - Solar Orbiter overview* https://www.esa.int/Science_Exploration/Space_Science/Solar_Orbiter/Solar_Orbiter_overview.
6. *About Hubble* https://science.nasa.gov/mission/hubble/overview/about-hubble/.
7. *ASTERIA (Arcsecond Space Telescope Enabling Research in Astrophysics)* https://www.jpl.nasa.gov/missions/arcsecond-space-telescope-enabling-research-in-astrophysics-asteria.
8. Nardello, M. *Optical subsystems of metis (multi element telescope for imaging and spectroscopy) on board of the solar orbiter mission* 2016 Jan 31. https://hdl.handle.net/11577/3426761.
9. Mancuso, Salvatore. Water production rate of comet C/1997 H2 (SOHO) near perihelion. *A & A* **578,** L7 (2015).
10. *CubeSat 101 Basic Concepts and Processes for First-Time CubeSat Developers* ().
11. *CubeSats in a nutshell* https://www.asc-csa.gc.ca/eng/satellites/cubesat/what-is-a-cubesat.asp#who.
12. Genet, R. *et al.* CubeSat Astronomical Telescops and Research in the 2020s. *Bulletin of the AAS* **51.** https://baas.aas.org/pub/2020n7i051 (Sept. 2019).

13. Shkolnik, E. L. On the verge of an astronomy CubeSat revolution. *Nature Astronomy* **2,** 374–378. ISSN: 2397-3366 (May 2018).

14. The CubeSat Program, C. P. S. *CubeSat Design Specification Rev. 14.1* (Feb. 2022).

15. Corso, A. J. *Appunti del corso "Elementi di Ottica e Applicazioni"*

16. Hecht, E. *OPTICS* (Pearson, 2017).